Geomicrobiology Journal (2015) **32**, 878–889

ISSN: 0149-0451 print / 1521-0529 online
DOI: 10.1080/01490451.2015.1017623

Taylor & Francis
Taylor & Francis Group

Secondary Mineral Formation During Ferrihydrite Reduction by *Shewanella oneidensis* MR-1 Depends on Incubation Vessel Orientation and Resulting Gradients of Cells, Fe^{2+} and Fe Minerals

URS DIPPON, CAROLINE SCHMIDT, SEBASTIAN BEHRENS, and ANDREAS KAPPLER*

Department of Geomicrobiology, Center for Applied Geosciences, University of Tübingen, Tübingen, Germany

Received November 2014, Accepted February 2015

In previous studies on microbial ferric iron (Fe(III)) reduction varying results regarding reduction rates and secondary mineral formation have been reported for almost identical conditions regarding temperature, pH, medium composition, Fe(III) mineral identity and bulk iron concentration. Here we show that in addition to physico-chemical parameters also geometric aspects, i.e., incubation orientation and dimension of cultivation vessels, influence the reduction rates and mineralogy. We incubated the Fe(III)-reducer *Shewanella oneidensis* MR-1 in test tubes at ferrihydrite (FH) concentrations of 1.3–50 mM either in vertical or horizontal orientation. Cells and minerals formed a pellet at the bottom of the tubes with different thicknesses at the same initial FH concentration depending on the incubation orientation. In vertically incubated tubes thick FH pellets were present at the bottom of the tubes and magnetite was formed in all setups with $\geq$2.5 mM initial FH. In tubes that were incubated horizontally no magnetite was formed in presence of $<$5 mM initial FH. Spatially resolved analysis of the supernatant and mineral sediment including voltammetric microelectrodes, Xray diffraction and Mössbauer spectroscopy revealed strong gradients of Fe^{2+} in both the aqueous supernatant and mineral pellets, whereas a heterogeneous distribution of cells and minerals in the sediment pellet was detected. The highest cell density and, consequently, the initiation of FH reduction was found at the mineral-supernatant interface. This study demonstrates that small changes in incubation conditions can significantly influence and even change the experimental results of geomicrobiological experiments.

Keywords: biogenic magnetite formation, incubation conditions, microbial Fe(III) mineral reduction

Introduction

Understanding and ultimately predicting secondary mineral formation during microbial transformation of iron minerals in the environment is of wide interest. It allows to better understand the evolution of redox conditions throughout Earth's history (Kendall et al. 2012; Posth et al. 2014), the coupling of biogeochemical cycles including the preservation of organic matter (Lalonde et al. 2012; Raiswell and Canfield 2012), and the fate of contaminants in soils and sediments (Benzerara et al. 2011; Borch et al. 2010; Vaughan and Lloyd 2011).

Dissimilatory iron(III)-reducing bacteria (DIRB) can use poorly soluble Fe(III) (oxyhydr)oxides as electron acceptor for respiration, which requires mechanisms for extracellular electron transfer (Melton et al. 2014). Electrons can be transferred by bacteria to iron(III) via direct contact with the mineral surface (Lovley and Phillips 1988) via endogenous electron shuttles produced by the bacteria (Lies et al. 2005; Marsili et al. 2008) via conductive pili (so-called nanowires), (Lovley et al. 2014; Pirbadian et al. 2014) or by natural redox-active organic compounds such as humic substances, sulfur species or even biochar (Jiang and Kappler 2008; Kappler et al. 2014; Lohmayer et al. 2014; Lovley et al. 1996; Okamoto et al. 2013; Roden et al. 2010).

Direct contact electron transfer, flavin production and electron shuttling by humic substances have been reported to be performed by *Shewanella oneidensis* MR-1, the Fe(III)-reducing strain used in this study. Common to all electron transfer pathways described is that short distances between Fe(III)-reducing cells and minerals are crucial or at least beneficial to allow efficient electron transfer. For strain *S. oneidensis* MR-1, no biomolecules are known that control the identity of the secondary minerals formed outside of the cell during Fe(III) mineral reduction. This is in contrast to magnetotactic bacteria, which exert a strong control over the

*Address correspondence to Andreas Kappler, Geomicrobiology, Center for Applied Geosciences, University of Tübingen, Sigwartstrasse 10, D-72076 Tübingen, Germany; Email: andreas.kappler@uni-tuebingen.de
Color versions for one or more of the figures in the article can be found online at www.tandfonline.com/ugmb.

intracellular formation of iron minerals (Bazylinski and Frankel 2004).

During Fe(III) mineral reduction by *S. oneidensis* MR-1, a number of secondary minerals such as goethite, magnetite, siderite or vivianite have been found and various factors controlling the identity of secondary minerals described (Piepenbrock et al. 2011). Direct iron mineral (trans)formation is strongly controlled by a number of physicochemical parameters, including thermodynamic and kinetic properties of the reaction system, as well as biological and physical settings and the design of the experimental setup (Figure 1) (Fredrickson et al. 1998; Fredrickson et al. 2003; Hansel et al. 2003; Lies et al. 2005; Piepenbrock et al. 2011; Zachara et al. 2002).

A systematic classification of these parameters leads to a hierarchical and successive control scheme on secondary mineral formation (Figure 1). The highest control level, indicated by level 1, is represented by the thermodynamic framework. This framework includes temperature, pH, local geochemistry on a microscopic scale and the interaction of the cells with reactive groups at the mineral surface. As a subsequent level the reaction kinetics (level II), including chemical and biological reaction rates as well as catalytic processes, control the secondary mineral formation.

Further control levels are biological factors (level III) and the physical framework (level IV). Biological factors comprise the influence of cell density, metabolic activity, nutrient and substrate availability on the mineral (trans)formation. The physical framework describes nonbiological influences, such as the spatial distribution of chemical species (i.e., formation of gradients), the accessibility of cells to the mineral surface and the presence and interactions of surface blocking agents (e.g., phosphate, humic substances). A final important parameter in this hierarchical control scheme is the design and choice of the experimental setup (level V), including shape and size of the incubation vessel, agitation disturbances and the incubation temperature as discussed in detail later in the present study.

All the factors mentioned above influence, either directly or indirectly, the identity of the mineral product of DIRB

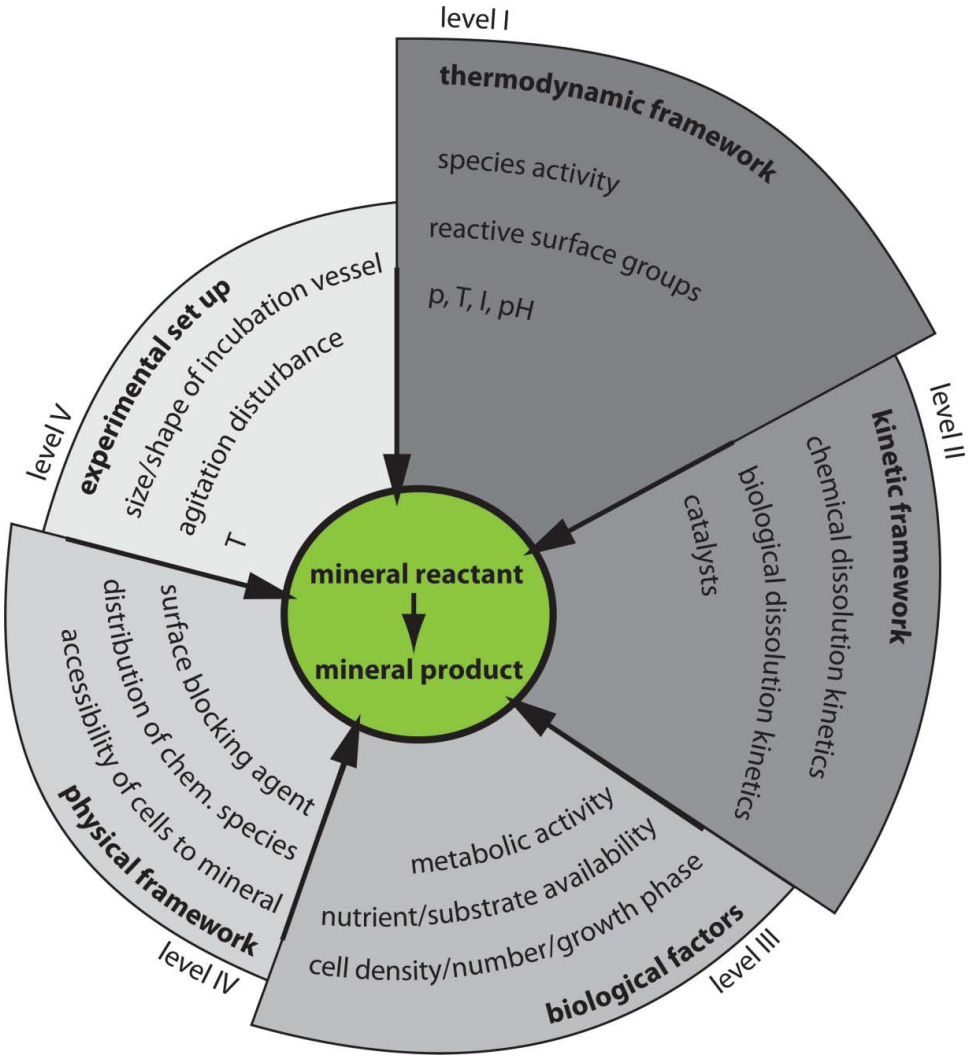

Fig. 1. Chemical, biological, physical and experimental factors influencing the secondary mineralization product of microbial Fe(III) mineral transformation.

activity, leading to various products depending on the parameter combination. In laboratory experiments mainly the control parameters that are comprised in levels III and IV (Figure 1) are applied to manipulate experimental conditions and to direct mineral formation. However, even under very similar conditions regarding temperature, pH, medium composition and initial Fe(III) concentration and Fe(III) mineral identity, the identity and quantities of the secondary minerals formed during Fe(III) reduction was shown to vary (Piepenbrock et al. 2011). In the present study we investigated systematically how the design and choice of the experimental setup (level V) affects iron mineral (trans)formation.

The goal was to determine how geometric factors, such as vessel incubation orientation and dimension/shape influence the local conditions in the experiment and ultimately control the mineralogy during microbial Fe(III) mineral reduction. While up-and downscaling of microbial reactors are always a challenge and often no linear behavior with respect to volume, cell growth and metabolic rates is observed, this is especially true for Fe(III)-mineral-reducing cultures, in which the iron minerals sediment rapidly and the major volume of the aqueous medium contains the dissolved electron donor (e.g., lactate or acetate) but lacks the electron acceptor. Experiments identical in bulk composition may therefore lead to different secondary minerals depending on the experimental scale and setup.

Therefore, we investigated the influence of incubation vessel orientation, dimension and heterogeneous distribution of cells and minerals on mineral transformation during ferrihydrite (FH) reduction by *Shewanella oneidensis* MR-1. Culture tubes were set up with identical cell numbers, nutrient and FH concentrations, either standing vertically or lying horizontally in the incubator either without disturbance or shaken once per day (Figure 2A).

Materials and Methods

Bacterial Culture

Shewanella oneidensis strain MR-1, originally isolated from Lake Oneida, New York, (Myers and Nealson 1988) was taken from a frozen stock kept at −80°C and streaked out oxically on Luria–Bertani (LB-medium) agar plates (10 gL^{-1} tryptone, 5 gL^{-1} yeast extract, 5 gL^{-1} NaCl and 12 gL^{-1} agar). LB-plates were incubated at 28°C for about 24 h and afterwards kept at 4°C for up to 7 days. One colony was transferred into 10 mL of anoxic freshwater medium (Hegler et al. 2008) amended with 20 mM lactate and 40 mM fumarate in a 21-mL culture tube. After 72 h of incubation at 28°C in the dark, 200 μL were transferred into a culture tube with freshwater medium. After another 24 h of incubation, cell concentration in the culture was determined by optical density (OD) measurements (660 nm). OD_{660} was calibrated against cell counts obtained by counting with a Thoma-chamber by light microscopy (Axioscope 2, Zeiss, Germany). The cultures were diluted to 2×10^7 cells mL^{-1} and 200 μL were used to inoculate the experiments.

Ferrihydrite (FH) Synthesis

FH was synthesized according to Cornell and Schwertmann (2003) and Piepenbrock et al. (2011) using a ca. 200 mM solution of $Fe(NO_3)_3 \cdot H_2O$ that was neutralized with 1 M KOH to a final pH of 7.2. After centrifugation and four washing steps with demineralized water, the wet solid was resuspended in water to an approximate concentration of 0.5 M Fe(III). The FH suspension was deoxygenized under vigorous stirring by alternating application of vacuum and N_2, autoclaved (20 min at 121°C) and then stored in the dark at 4°C.

Experimental Setup

All experiments were conducted at 28°C in the dark in anoxic LML medium. LML medium contained 0.2 g L^{-1} yeast extract, 0.1 g L^{-1} peptone and 22 mM $NaHCO_3$ buffer adjusted to pH 7.0–7.1. Test tubes with a volume of 13.5 or 21 mL were used with 6 or 10 mL of medium, respectively. Anoxic FH stock suspension was added to the tubes to final concentrations of 1.3–50 mM using syringes after the headspace was flushed with N_2/CO_2 (90:10) and all vessels were closed with butyl rubber stoppers. Finally, all tubes except sterile controls were inoculated with *S. oneidensis* using syringes as described above. The incubation vessels were stored in different orientations: vertically, horizontally, and horizontally shaken once per day. For analysis by voltammetric electrodes, 13.5 mL test tubes with 50 mM FH were completely filled with medium and incubated without headspace to allow sufficient immersion of the counter and reference electrodes. Table 1 provides an overview of all setups.

Cell Number Quantification by qPCR

Cells in the experimental setup were quantified by qPCR as described in the supporting information.

Analytical Techniques

Lactate and acetate were quantified by HPLC (Shimadzu, Kyoto, Japan) equipped with an Aminex HPX 87H column (BioRad, Hercules, USA), a refractive index detector for lactate and a diode array detector for acetate. For bulk analysis of Fe concentrations and speciation, the incubation tubes were homogenized by vigorous shaking and samples were taken anoxically using a syringe with a needle. Samples were immediately stabilized in 1M HCl to avoid oxidation of Fe (II). For Fe distribution profiles, the tubes were either mounted on a micromanipulator for Fe species identification and quantification using voltammetric microelectrodes or the tubes were frozen at −28°C and sliced inside an anoxic glove box as described for cell quantification. The cut ice cores were then thawed and subsamples were dissolved in 1M HCl for analysis. Fe(II) was quantified photometrically by the ferrozine assay. (Stookey 1970) For Fe_{tot} measurements, Fe(III) was reduced to Fe(II) prior to quantification according to (Kappler and Brune 2002).

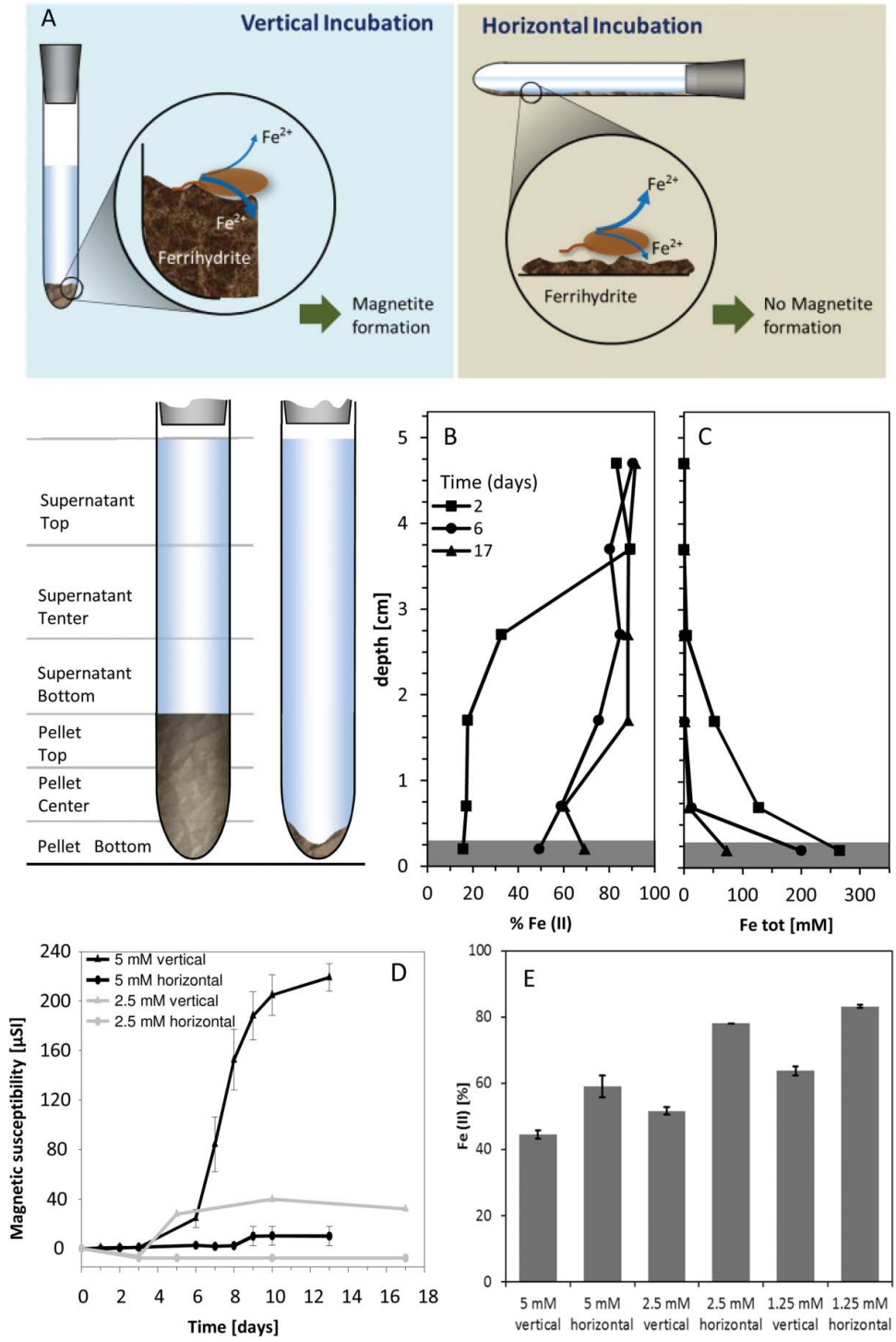

Fig. 2. (A) Conceptual drawing of the experimental setup. Culture tubes with initially 1.3–50 mM ferrihydrite (FH) were incubated with *Shewanella oneidensis* MR-1 either horizontally or vertically. Depending on incubation orientation and FH concentration, thick FH pellets (sedimented FH minerals) formed or the FH was distributed in a thin layer in the tubes. (B) Spatial distribution of Fe(II)/Fe(tot) ratios (1 M HCl extractable Fe) in 21 ml culture tubes with 2.5 mM FH, inoculated with MR-1 and incubated vertically for 2, 6 and 17 days, respectively. Gray shaded area represents samples taken from the mineral pellet. (C) Fe(tot) concentration for the same tubes as described in panel B. (D) Development of magnetic susceptibility over time in culture tubes incubated either vertically or horizontally for bulk FH concentrations of 2.5 and 5 mM. Horizontal tubes were shaken once per day before measurement while vertical tubes were not. Error bars indicate range of values for duplicate tubes. (E) Extent of total Fe(II) formed from microbial Fe (III) reduction in 21 mL tubes containing 1.3, 2.5 or 5 mM FH incubated either vertically or horizontally for 8 days without shaking.

Table 1. Mineral transformation during reduction of different concentrations of ferrihydrite by *Shewanella oneidensis* MR-1 depending on the incubation orientation of culture tubes

Volume of tube / medium [mL]	Type of incubation	Amount of ferrihydrite [mmol]	Concentration of ferrihydrite [mM]	Formation of magnetite
13.5/13.5	Vertical	0.68	50	Yes
13.5 / 6	Vertical	0.05	8.77	Yes
13.5 / 6	Vertical	0.0285	5	Yes
13.5 / 6	Vertical	0.0162	2.85	Yes
13.5 / 6	Vertical	0.0143	2.5	No
13.5 / 6	Vertical	0.0074	1.3	No
21 / 10	Vertical	0.5	50	Yes
21 / 10	Vertical	0.05	5	Yes
21 / 10	Vertical	0.0285	2.85	Yes
21 / 10	Vertical	0.025	2.5	Yes[a]
21 / 10	Vertical	0.013	1.3	No
21 / 10	Horizontal	0.05	5	Yes
21 / 10 shaken	Horizontal	0.05	5	No[b]
21 / 10	Horizontal	0.0285	2.85	No
21 / 10	Horizontal	0.025	2.5	No
21 / 10 shaken	Horizontal	0.025	2.5	No
21 / 10	Horizontal	0.013	1.3	No

[a]Magnetite is not the main phase, magnetic susceptibility is only 30% of the expected intensity.
[b]Only weak traces of magnetite found, magnetic susceptibility is only 5% compared to vertical incubation.
The minerals were analyzed by magnetic susceptibility measurements after 10 days of incubation.

Cyclic voltammetry microelectrode measurements were performed using an AIS DLK-100 potentiostat (Analytical Instrument Systems, Flemington, USA) set to a voltage range 1.8 to 0.1 V. The working electrodes were custom made with a tip diameter of 100μm and a polished Au-Hg coating. The counterelectrode was made of platinum and as reference a standard Ag/AgCl glass electrode was used (Brendel and Luther 1995). Measurements were performed at 5 mm depth intervals in the medium and every 3 mm in the mineral pellet.

Minerals were analyzed by Mössbauer spectroscopy as described in Dippon et al. (2012) and by powder X-ray diffraction (XRD) as described in the supporting information. Magnetic susceptibility was used as noninvasive proxy for magnetite formation. (Porsch et al. 2010) Magnetic susceptibility was measured on a KLY-3 kappa bridge (Agico Co., Brno, Czech Republic) using the culture tubes without sampling. All tubes were analyzed twice and measurements of blanks were subtracted during data processing to correct for sensitivity fluctuations of the KLY-3 device. Vertically incubated tubes were measured upright without any disturbance, while horizontally incubated tubes were mixed before the measurements.

Results

Rates and Extent of Ferrihydrite (FH) Reduction Depending on Vessel Incubation Orientation

The rates and extent of microbial FH reduction by *Shewanella oneidensis* MR-1 were influenced by shaking, and the incubation orientation of the glass tubes containing Fe(III)-reducing MR-1 cells, lactate as electron donor and varying concentrations of FH as electron acceptor. For the concentrations of 1.3–5 mM FH, the horizontally incubated tubes (nonshaken) showed faster rates and higher extents of FH reduction compared to the vertically incubated nonshaken setups containing the same FH concentrations (Figure 2E). Quantification of total Fe(II) after 8 days of incubation showed that the extent of reduction in horizontally incubated tubes was higher by 31–51% compared to vertically incubated tubes with the same FH concentration (Figure 2E).

We also observed that with decreasing FH concentration, the extent of reduction increased. In vertically incubated tubes that initially contained 5 mM FH, 44.4 $\pm$ 1.3% Fe(III) was reduced to Fe(II) within 8 days, while 63.7 $\pm$ 1.3% Fe (III) was reduced in tubes with an initial FH concentration of 1.3 mM. In horizontally incubated tubes the extent of reduction after 8 days of incubation was significantly higher with 59.1 $\pm$ 3.2% reduction for initial FH concentration of 5 mM and 83.1 $\pm$ 0.4% reduction for an initial FH concentration of 1.3 mM.

Spatial Distribution of Fe and Redox Speciation in Mineral Pellet and Aqueous Supernatant

Tubes containing medium, ferrihydrite and MR-1 cells were frozen for wet-chemical analysis. We found that depending on the initial FH concentration, between 81–97% of the total iron was present in the iron-mineral-cell sediment at the bottom of the tube, which we termed "mineral pellet" (Figure 2C). The remaining Fe was present in the aqueous supernatant overlaying the mineral pellet probably including colloidal Fe(III) particles, dissolved Fe(III)-organo complexes as well as dissolved Fe(II) (Figures 2B, 2C for 2.5 mM

FH, 3A, 3B for 50 mM FH). For vertically incubated non-shaken tubes distinct gradients in the distribution of Fe(II) and Fe(III) and in Fe(II)/Fe(tot) ratios within the supernatant were observed for all FH concentrations (Figures 2B, 2C, 3A, 3B).

The gradients changed over incubation time, in tubes with 2.5 mM FH they were steepest during the first days of incubation with low Fe(II) in the mineral pellet, and in the supernatant directly above the pellet while the Fe(II) fraction (relative to the total amount of Fe present) was much higher (>80%) in the upper part of the aqueous supernatant. Over time (within the following days) the Fe(II) distribution was more homogeneous throughout the tubes (Figure 2B). The data showed that the supernatant was dominated throughout the experiment by Fe(II) but always contained some Fe(III), while the mineral pellet slowly transformed from a pure Fe (III) mineral to Fe(II)-containing mineral phases during the course of the incubation.

To obtain a more detailed view of the spatial resolution of different Fe redox-species, we used voltammetric microelectrodes. Analysis of vertically incubated tubes after 2 and 9 days of incubation showed two distinct current signals at around −1.1 to −1.4 mV and −0.4 to −0.7 mV which were assigned to dissolved Fe(II) and Fe(III)-organo complexes (Figure 4). (Jones et al. 2010; Luther et al. 2008) The voltammograms showed a relative increase in concentration for both Fe species from the top of the supernatant toward the mineral pellet surface. When the electrode touched the surface, the potential of the Fe(III) peaks shifted, indicating a change in the Fe redox-species interacting with the electrode. The concentration gradients of Fe(II) in the supernatant were more distinct after 2 days (Figure 4A) compared to 9 days where high Fe (II) levels were recorded throughout the supernatant (Figure 4B). In contrast, the concentration of Fe(III)-organo complexes showed both a stronger gradient and higher concentrations after 9 days of incubation compared to 2 days (Figure 4B). Measurements in sterile controls that contained FH and lactate but no MR-1 cells did neither show signals for dissolved Fe(II) nor for dissolved Fe(III)-organo complexes (Figure SI1).

Spatial Distribution of MR-1 Cells, Lactate and Acetate in Mineral Pellet and Supernatant

Since the reduction of Fe(III) and formation of Fe(II) is directly linked to the activity of Fe(III)-reducing bacteria and the electron donor availability, we quantified both cell numbers and concentrations of lactate (electron donor, i.e., the source of electrons for Fe(III) reduction) and acetate, i.e., the product of lactate oxidation) in different layers of the mineral pellet and the aqueous supernatant for tubes with 50 mM initial FH incubated vertically. We found that after 5 days, most of the MR-1 cells were located in the upper and central parts of the mineral pellet (Figure 3C). Although 3.6×10^5–1.3×10^6 cells per g medium were planktonic, the cell density in the upper part of the pellet was approximately 6.3×10^8 cells per g mineral sludge (wet weight) and dropped to 3.7×10^5 cell per g sludge in the lower part of the mineral pellet.

The concentrations of lactate and acetate showed strong gradients in tubes incubated for 3 and 7 days. After 3 days we observed 2.9–5 mM lactate in the supernatant with the lowest concentration (2.9 mM) at the top of the supernatant and the highest concentration (5 mM) in the liquid right above the mineral pellet. Within the mineral pellet the lactate was homogeneously distributed with a concentration of 6.4–6.6 mM (Figures SI 2A). Acetate showed a similar distribution with slightly lower concentrations.

After 7 days' of incubation, the lactate and acetate gradients had changed and we observed steeper gradients between the upper supernatant and the minerals pellet compared to the day 3 samples with lactate values ranging from 2–4.3 mM (top of supernatant to bottom of supernatant) to 9 mM (pellet surface) and 4.9 mM at the bottom of the pellet

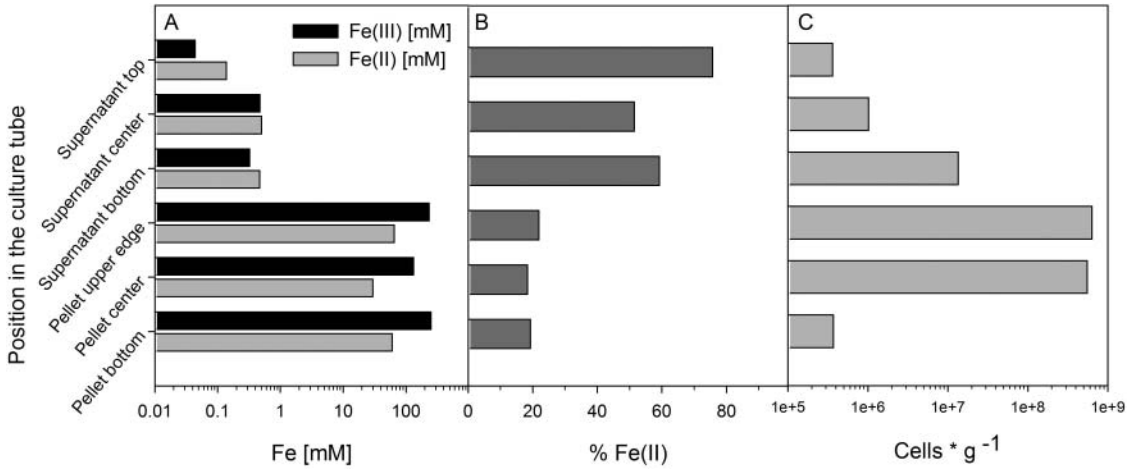

Fig. 3. Distribution of Fe redox-species and microbial cells in vertically incubated culture tubes with 50 mM ferrihydrite after 5 days of incubation at 28°C. (A) Concentrations of total Fe(II) and total Fe(III) determined by 1 M HCl-extraction. Most of the iron is present in the pellet (please note the logarithmic scale). (B) Proportion of total Fe(II) in terms of total iron concentration. (C) Distribution of *Shewanella oneidensis* MR-1 cells after 5 days of incubation quantified by qPCR (please note the logarithmic scale).

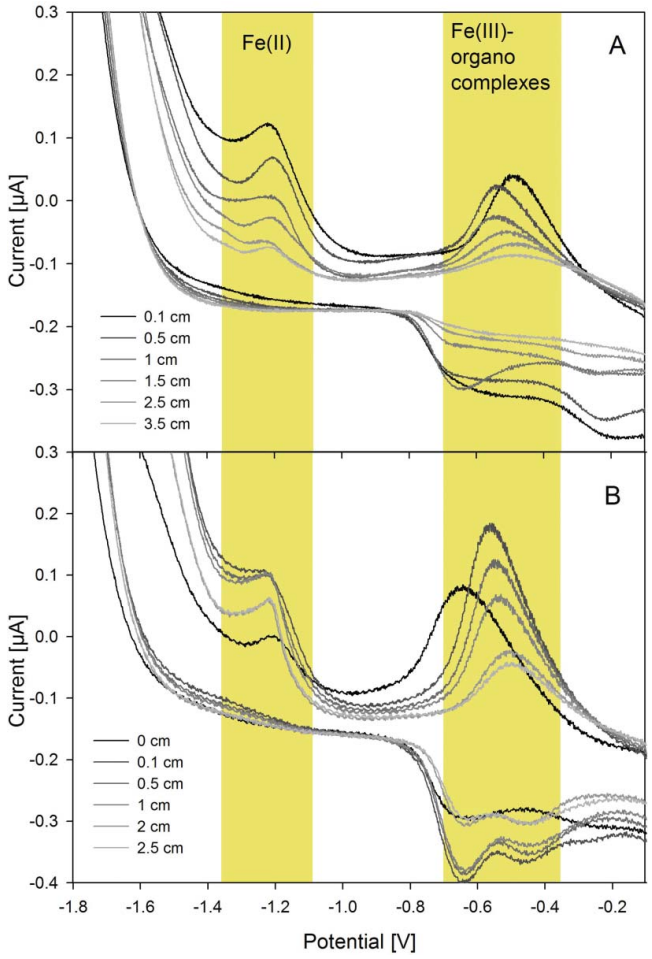

Fig. 4. Voltammograms measured with microelectrodes in culture tubes (5 mM ferrihydrite) incubated vertically with MR-1 for (A) 2 days and (B) 9 days. Distances in cm give the height above the pellet surface where 0 is the pellet surface. The signal for dissolved Fe^{2+} is in the range of −1.4 to −1.1 V and for dissolved Fe(III)-organo complex in the range of −0.7 to −0.4 V (yellow highlighted areas). The concentrations are proportional to peak height and decrease with increasing distance from the mineral pellet for both time points with exception of the measurement in the pellet (0 cm) after 9 days.

(Figure SI 2B). The acetate concentration showed a similar distribution, but with a less pronounced decrease in concentration towards the bottom of the pellet (Figure SI 2B). Sterile controls indicated that 0.01 mM of lactate sorbed per 1 mM of FH (Figure SI 3).

Mineral Identity and Distribution During Microbial Ferrihydrite Reduction

Visual observation of the microbially-active tubes containing FH and MR-1 revealed that within 3–6 days a color gradient developed from the initial homogeneously reddish-brown mineral pellet to black at the top, and brown at the bottom, of the pellet (Figure SI 4). After 10 days the color gradient disappeared and the mineral pellet appeared homogeneously black.

We used magnetic susceptibility analysis, XRD and Mössbauer spectroscopy to identify the Fe minerals formed during FH reduction. Magnetic susceptibility measurements showed that magnetite formed in all vertically incubated culture tubes containing at least 2.85 mM FH (Table 1, Figure 2D). For initial FH concentrations of 2.5 mM magnetite was formed only in 21 mL tubes containing 10 mL medium but not in smaller tubes containing 6 mL of medium. Horizontally incubated tubes (10 mL medium), which were not shaken during incubation showed magnetite formation only in the presence of at least 5 mM FH. When tubes containing 5 mM FH were shaken once per day only small traces of magnetite were formed compared to nonshaken tubes (Figure 2D, Table 1). In summary, this suggests that magnetite formation depends on local concentrations of FH, i.e., the thickness of the FH pellet that depends in turn on the incubation orientation of the experimental vessels and on the total FH concentration but also on the volume of medium and thus the total amount of FH sedimenting from the medium.

XRD and Mössbauer spectroscopy were used to identify the minerals formed during FH reduction. Due to the low amount of sample material, spatially resolved mineralogical analysis was only possible for the setups containing 50 mM of FH. XRD and Mössbauer spectroscopy of 50-mM-FH-tubes that were incubated vertically showed a transformation of FH to goethite and magnetite during FH reduction. The transformation of FH generally started in the upper layer of the mineral pellet. After 3 days of incubation, the top part of the pellet consisted of a mixture of magnetite and goethite (Figure 5A). Widened reflections in the X-ray diffractograms as well as in 140K Mössbauer spectrograms suggest a small particle size and low crystallinity (Figures 5A, 5C).

In the material taken from the center part of the pellet, the magnetite reflections in X-ray diffractograms were much weaker and completely absent in the lower part of the pellet (Figure 5A). The minerals in the lower part of the pellet showed only weak X-ray reflections after 3 days, suggesting the presence of mainly X-ray amorphous minerals such as FH (Figure 5A). The presence of remaining FH after 3 days in the bottom of the pellet was confirmed by Mössbauer spectroscopy, which showed the paramagnetic contribution of the sample increasing from 18 to 55% of spectral area from the top to the bottom of the pellet. The paramagnetic signal in the Mössbauer spectra contains FH and transition forms to more crystalline structures such as goethite and magnetite (Figure 5C).

The magnetically split material, which can be attributed to more crystalline material is expected to appear as one sextet for goethite and two sextets for magnetite in the Mössbauer spectra based on the XRD analysis (Figure 5C). Even the more crystalline minerals showed widened peaks with significant "innerline broadening" leading to overlapping features between the different minerals. The strong "innerline broadening" and the resulting lack of sharp peaks and shoulders indicate magnetic relaxation found in small particles and low crystalline materials. Therefore, the magnetically split material, covering 45–82% of spectral area was modeled as a sum of only two sextets, a separate quantification of magnetite and goethite was not possible for this time point (Table SI 1).

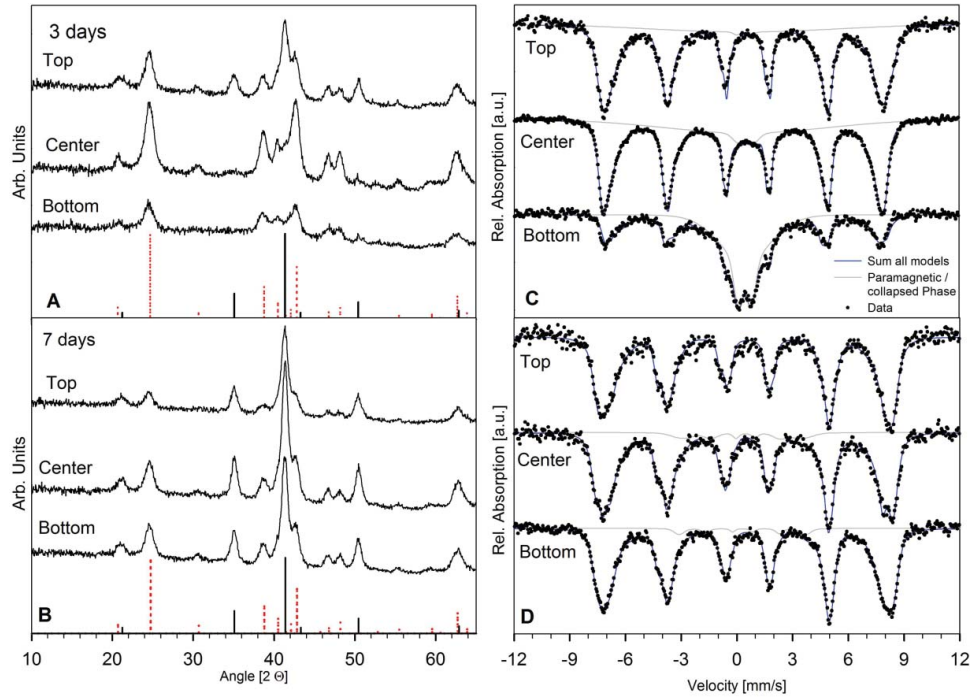

Fig. 5. Mineralogical characterization of iron minerals formed within 3 and 7 days of ferrihydrite reduction (50 mM) in vertically incubated tubes by *Shewanella oneidensis* MR-1. The samples were taken from three different depths and the labels top, center and bottom describe the origin of the sample material within the mineral pellet. A&B: Powder X-ray diffractograms of minerals formed after 3 (A) and 7 days (B). References: dashed lines goethite, solid lines magnetite. C&D: Mössbauer spectra of the same samples as used for XRD, recorded at 140K. Black dots: data, blue line: overall fit, grey line: model for paramagnetic doublet (3 days) and collapsed sextet (7 days), respectively.

After 7 days of incubation, XRD indicated a mixture of magnetite and goethite in all three layers (Figure 5B). Mössbauer spectroscopy suggested a higher crystallinity in all three layers, with no detectable paramagnetic phases. Similar to the 3-day samples, an innerline broadening was observed for the sextets, but weaker than before. The three analyzed layers consisted almost completely of goethite and magnetite. The top and bottom layer showed a higher magnetite contribution of 55–57% (spectral area) compared to the sample from the center with 45%. The remaining area of the Mössbauer spectrum was modeled as goethite plus in the center and bottom layer a collapsed sextet which covers 4–6% of spectral area and represents a Fe(III) dominated transition phase of FH to more crystalline material (Figure 5D and Table SI 1).

Discussion

Microbial reduction of Fe(III) minerals and secondary mineral transformation has consequences for many biogeochemical element cycles and controls the fate of pollutants and nutrients in the environment (Borch et al. 2010; Muehe et al. 2013a; Muehe et al. 2013b). In many cases the identity of the minerals produced is the key property that determines the redox activity and sorption capacity of the solids (Elsner et al. 2004). Our present study showed that in laboratory experiments designed to simulate and understand environmental mineral (trans)formation not only geochemical conditions and parameters such as temperature and cell numbers control the rates of mineral transformation and thus the identity of the minerals.

We showed that the choice of the experimental vessel dimension and orientation during incubation led to the sedimentation of either thin layers of FH (horizontally incubated tubes) or to thick, dense pellets (vertically incubated tubes) and ultimately controlled the reduction rates and the identity of the minerals formed under otherwise identical starting conditions, i.e., at identical total ferrihydrite concentrations. In the following sections we first discuss how in the experimental tubes that contain minerals suspended in liquid media plus nutrients and organic substrates at the time of setup distinct microenvironments form shortly after the setup.

This discussion includes how gradients of substrate and Fe^{2+} develop and how the reaction rates and the extent of FH reduction differ depending on vessel size and orientation during incubation. In the second section we discuss the geochemical Fe-species that are distributed heterogeneously in the sedimented mineral pellet and supernatant forming distinct microenvironments. In the third part we present how this leads to the formation and distribution of different Fe minerals within the same experimental system and what implications this has for the design of experiments for mineral (trans-)formation studies.

Variations in Lactate, Cell Distributions and Rates and Extent of FH Reduction

Our experiments showed that the Fe(III) reduction rates are strongly influenced by the distribution of FH in the incubation tubes based on how the vessels are stored in the incubator during the experiments. When FH was distributed in a thin layer in horizontally incubated tubes, faster reduction rates and a higher extent of reduction have been observed compared to vertical incubation where the FH aggregated in a thick pellet (Figure 2E). This suggests a lower metabolic activity of the MR-1 cells in the thick pellets, which were probably limited by the availability of either the electron donor (lactate) or acceptor (FH) due to the dense packing of the thick mineral pellet.

Additionally to the dense mineral packing, the fact that most cells were concentrated in a relatively small volume on the top of the pellet may have led to limitations in electron transfer efficiency to FH compared to horizontal incubation. Due to the different sedimentation rates of the heavy FH particles compared to the lighter cells, an inhomogeneous distribution of cells is most probably already present directly after inoculation. However, since MR-1 is a motile bacterium (Myers and Nealson 1988), we expect the cells to be able to move towards preferential locations where they find optimal conditions for Fe(III) reduction and growth during the incubation. Localities where high cell densities were observed after several days of incubation, therefore, probably provided the most favorable conditions for growth, where the availability of lactate and FH were highest, i.e., at the interface of the FH pellet and the supernatant. And indeed, cell concentrations strongly increased over the course of the experiment especially in the upper part of the pellet, suggesting favorable conditions for growth at the interface between supernatant and mineral pellet (Figure 3C).

Since in vertically incubated setups most cells were found in the upper part of the mineral pellet, we expected reduced lactate and increased acetate concentrations at the pellet surface compared to the upper water column in the tubes due to efficient lactate consumption of the cells in the top part of the pellet. In contrast to our expectation, lactate quantification did not show any depletion (Figure SI 1). In fact, after 3 days of incubation the lactate concentration in the pore water of the pellet was even higher compared to the supernatant. This distribution profile was even more pronounced after 7 days of incubation (Figure SI 1). The accumulation of lactate within the cell-mineral pellet over time could be due to sorption of lactate to the iron minerals. Indeed, sterile control experiments showed that 0.0112 mM lactate/mM FH were sorbed to FH (Figure SI 3).

Considering a FH concentration of about 160–310 mM Fe (tot) in the pellet (Figure 3A), a maximum of 1.8 to 3.5 mM lactate are expected to sorb assuming that the sorption capacity of the minerals did not change significantly during microbial reduction and secondary mineral formation. Therefore, the elevated lactate concentrations in the pellets of microbially active setups after 3 days of incubation can be explained by lactate sorption to the Fe minerals. Additionally, it cannot be ruled out that MR-1 cells stored lactate internally that is released during sample preparation for lactate HPLC analysis (that includes freezing and thawing of the cell-mineral pellets).

After 7 days of incubation, the lactate concentration in the supernatant decreased to 2.0–4.3 mM, consistent with the consumption of lactate by MR-1 during FH reduction. Surprisingly, the concentration in the pellet increased to 4.7–9.2 mM, with the highest concentration of 9.2 mM in the upper part of the mineral pellet, where also the highest cell density was found (Figure 3C and Figure SI 2B). We expected to find the lowest lactate concentration in the upper part of the pellet due to consumption by MR-1; however, in our experiments, the highest concentration was found in this layer. Release of lactate stored in MR-1 cells occurred probably during sample preparation which included freezing of the samples, but is unlikely to be responsible alone for the high concentration of lactate measured since this would require lactate concentrations of >1M within the cells. Therefore, the secondary Fe minerals formed in this section upon 7 days of incubation most likely had a much higher sorption capacity for lactate than the initial FH.

Acetate is the metabolic product of lactate oxidation coupled to FH reduction by MR-1 and the increasing acetate concentration as a function of time in the region of highest cell density correlates with the increasing cell populations shown by qPCR quantification in the same layer (Figure 3C and Figure SI 2B).

In summary, these observations suggest that microbial Fe (III) reduction in our experiments was limited mainly by the accessibility of the FH mineral surface for electron transfer and not by the availability of the electron donor, i.e., lactate (Amstaetter et al. 2012; Fredrickson et al. 2003; Hansel et al. 2003; Zachara et al. 2002). The accessibility of the FH for the bacteria correlated with the different thickness and corresponding density of the mineral pellet forming different microenvironments depending on the total amount of FH in the tube and the incubation orientation. This led to different FH reduction and microbial growth rates in the respective microenvironments and thus spatial differences of Fe(II) supply rates.

Distribution of Fe Redox-Species in Pellets and Supernatants of Ferrihydrite Reduction Experiments

During microbial FH reduction, mixed valent Fe minerals, dissolved Fe(II) and Fe(III)-organo complexes were formed (Figure 4). Since no Fe(III)-organo complexes were found in sterile controls, the formation of these complexes can be attributed to the activity of MR1. Similar Fe(III)-organo complexes have been described previously for experiments with *Shewanella putrefaciens* (Jones et al. 2010; Taillefert et al. 2007). Furthermore, Fe(III)-organo complexes have been found in various suboxic and anoxic sediments (Luther et al. 1996; Luther et al. 2008; Taillefert et al. 2000; Taillefert et al. 2002).

In our experiments, relative concentrations of Fe(III)-organo complexes showed a clear gradient with the highest concentration at the pellet surface (Figure 4), where also the highest number of cells was present (Figure 3C), which

decreased towards the top of the supernatant after both 2 and 9 days of incubation. Additionally, the peak positions for Fe (III)-organo complexes in the voltammograms shifted to lower potentials the closer the electrode moved to the surface of the mineral pellet. When the electrode hit the mineral surface, the potential changed again (Figure 4) indicating that the Fe(III) species (probably including Fe(III) complexes/colloids) interacting with the electrode had a different composition and/or properties in the pellet and supernatant.

Similar changes in peak position were observed during aging of synthetic Fe(III)-organo complexes, for *S. putrefaciens* cultures during aging and for combinations of FH with different alternative electron acceptors in experiments with *S. oneidensis* MR-1 (Jones et al. 2010; Taillefert et al. 2000; Taillefert et al. 2007). Besides different properties of the Fe (III)-complexes, also their concentration can influence the peak position due to colloid aggregation processes (Taillefert et al. 2007). Therefore, the incubation geometry controlled the heterogeneous distribution of MR-1 cells which lead to the localized formation of Fe(III)-organo complexes in the area of highest cell concentration, i.e., the top layer of the pellet. The complex concentration in turn controls the local amount and activity of dissolved Fe(III) which can ultimately govern mineral (trans-)formation.

Dissolved Fe(II) showed in general a similar distribution pattern as the Fe(III)-organo complexes. The Fe(II) gradients were steepest after 2 days of incubation and more homogeneous after 9 days of incubation (Figure 4B). This observation can be explained by a higher mobility of dissolved Fe(II) compared to the Fe(III)-organo complexes leading to equilibration over time, which was also evident from wet chemical extractions (Figure 2B) where the Fe(II) front moved upwards from the pellet. Additionally, the Fe(II) concentration in the pellet detected by voltammetric electrodes drops abruptly, indicating that Fe(II) found in the wet chemical extractions is sorbed or bound structurally and thus not detectable by the voltammetric electrodes (Figure 4) (Taillefert et al. 2000).

Identity and Spatial Distribution of Fe Minerals in Ferrihydrite Reduction Experiments

We distinguished nonmagnetic mineral products and magnetite in all our experiments using magnetic susceptibility measurements (Porsch et al. 2010; Porsch et al. 2014). Magnetite was formed in horizontally incubated tubes shaken once per day for bulk FH concentrations >5 mM while in vertical, nonshaken tubes magnetite was formed even at 2.5 mM bulk FH concentration. The difference in mineral formation can be explained by the sedimentation of the FH, which either formed a thin layer or a compact pellet, providing very different environments for cell growth and mineral formation in terms of FH accessibility, nutrient supply and accumulation of Fe(II). The variations in incubation orientation provided different growth conditions for the cells in each setup, but also within the same tubes, spatially distinct regions, "microenvironments" developed. Planktonic cells are exposed to different conditions compared to cells at the mineral pellet-supernatant interface or in the pore space of the mineral pellet.

For setups with 50 mM FH we conducted spatially resolved mineral identification by XRD and Mössbauer spectroscopy, which showed the formation of magnetite and goethite at different depths of the mineral pellet over time. The mineral transformation started in the upper part of the pellet where the cell density was highest, leading to a goethite/magnetite mixture while in the lower part of the pellet FH and goethite were dominating after 3 days. After 7 days, no paramagnetic components were present in the Mössbauer spectra, indicating an increased crystallinity. At this time point, magnetite was found in all layers of the pellet (Figure 5). These results are well in line with data reported by Piepenbrock et al. (2011) who showed that a certain $Fe(II)/Fe_{tot}$ ratio was necessary to trigger magnetite formation.

We could show that not bulk but local concentrations of cells, organic substrates and FH as well as resulting profiles of Fe(II) and Fe(III) are directing mineral formation. Our results suggest that the heterogeneity of geomicrobiological laboratory batch experiments influence the resulting mineralogy. This means that already small differences in handling of the experimental vessels or shaking due to transport can change the identity of the final mineral products.

Heterogeneity in terms of Fe(II) formation, electron acceptor and donor supply, and pH on a nm-to μm-scale in the vicinity of cells is relevant for understanding and analysis environmental mineral transformation and the production of biominerals (Coker et al. 2012; Hegler et al. 2010; Miot et al. 2014; Pearce et al. 2012). We showed that gradients on a mm-scale exist with zones of high cell concentrations and distinct chemical environments. Our data suggest that when comparing studies on the effect of reactive biogenic Fe minerals on contaminant mobilization, immobilization and degradation (Borch et al. 2010; Cerrato et al. 2013; Hohmann et al. 2010; Islam et al. 2004; Muehe et al. 2013c; Tufano and Fendorf 2008; Veeramani et al. 2011), in addition to the chemical and biochemical parameters such as Fe(III)/Fe(II) concentration and bulk reduction rates, it is necessary to consider the design of the experimental setups. This includes the orientation of the reaction vessels as well as the absolute volumes of the experimental setups leading to differences in spatial distribution of microbial cells and main iron redox species as well as compounds such as electron shuttles or complexing agents produced by the bacteria.

Acknowledgments

We would like to thank James Byrne for XRD measurements, Karin Stögerer for help with cell quantification and Greg Druschel for valuable advice concerning the use of voltammetric electrodes. This work was supported by a Margarete-von-Wrangell Habilitationsstipendium and a FIMIN travel grant to C.S. and by a BMBF "IPSWaT" PhD fellowship to U.D.

Funding

This work was supported by a Margarete-von-Wrangell Habilitationsstipendium and a FIMIN travel grant to C.S. and by a BMBF "IPSWaT" PhD fellowship to U.D.

Supplemental Material

Supplemental data for this article can be accessed on the publisher's webstie. Including description of cell number quantification by qPCR and mineral analysis by XRD, Figure SI 1 showing sterile controls for voltammetric microelectrode measurements, Figure SI 2 showing lactate and acetate distribution, Figure SI 3 showing sorption of lactate to ferrihydrite, Figure SI 4 showing images of mineral pellets, and Table SI 1 summarizing Mössbauer modeling data. http://www.tandfonline.com/UGMB

References

Amstaetter K, Borch T, Kappler A. 2012. Influence of humic acid imposed changes of ferrihydrite aggregation on microbial Fe(III) reduction. Geochim Cosmochim Acta 85:326–341.

Bazylinski DA, Frankel RB. 2004. Magnetosome formation in prokaryotes. Nat Rev Micro 2:217–230.

Benzerara K, Miot J, Morin G, Ona-Nguema G, Skouri-Panet F, Ferard C. 2011. Significance, mechanisms and environmental implications of microbial biomineralization. Compt Rendus Geosci 343:160–167.

Borch T, Kretzschmar R, Kappler A, Van Cappellen P, Ginder-Vogel M, Voegelin A, Campbell K. 2010. Biogeochemical redox processes and their impact on contaminant dynamics. Environ Sci Technol 44:15–23.

Brendel PJ, Luther GWI. 1995. Development of a gold amalgam voltammetric microelectrode for the determination of dissolved Fe, Mn, O_2, and S (-II) in porewaters of marine and freshwater sediments. Environ Sci Technol 29:751–761.

Cerrato JM, Ashner MN, Alessi DS, Lezama-Pacheco JS, Bernier-Latmani R, Bargar JR, Giammar DE. 2013. Relative reactivity of biogenic and chemogenic uraninite and biogenic noncrystalline U(IV). Environ Sci Technol 47(17):8709–8714.

Coker V, Byrne J, Telling N, Van der Laan G, Lloyd J, Hitchcock AP, Wang J, Pattrick RAD. 2012. Characterisation of the dissimilatory reduction of Fe (III)−oxyhydroxide at the microbe–mineral interface: the application of STXM–XMCD. Geobiology 10:347–354.

Cornell RM, Schwertmann U. 2003. The Iron Oxides: Structure, Properties, Reactions, Occurrence and Uses, 2nd ed. Weinheim: Wiley-VCH.

Dippon U, Pantke C, Porsch K, Larese-Casanova P, Kappler A. 2012. Potential function of added minerals as nucleation sites and effect of humic substances on mineral formation by the nitrate-reducing Fe(II)-oxidizer *Acidovorax* sp. BoFeN1. Environ Sci Technol 46:6556–6565.

Elsner M, Schwarzenbach RP, Haderlein SB. 2004. Reactivity of Fe(II)-bearing minerals toward reductive transformation of organic contaminants. Environ Sci Technol 38:799–807.

Fredrickson JK, Kota S, Kukkadapu RK, Liu C, Zachara JM. 2003. Influence of electron donor/acceptor concentrations on hydrous ferric oxide (HFO) bioreduction. Biodegradation 14:91–103.

Fredrickson JK, Zachara JM, Kennedy DW, Dong H, Onstott TC, Hinman NW, Li S-m. 1998. Biogenic iron mineralization accompanying the dissimilatory reduction of hydrous ferric oxide by a groundwater bacterium. Geochim Cosmochim Acta 62:3239–3257.

Hansel CM, Benner SG, Neiss J, Dohnalkova A, Kukkadapu RK, Fendorf S. 2003. Secondary mineralization pathways induced by dissimilatory iron reduction of ferrihydrite under advective flow. Geochim Cosmochim Acta 67:2977–2992.

Hegler F, Posth NR, Jiang J, Kappler A. 2008. Physiology of phototrophic iron(II)-oxidizing bacteria: implications for modern and ancient environments. FEMS Microbiol Ecol 66:250–260.

Hegler F, Schmidt C, Schwarz H, Kappler A. 2010. Does a low-pH microenvironment around phototrophic FeII-oxidizing bacteria prevent cell encrustation by FeIII minerals? FEMS Microbiol Ecol 74:592–600.

Hohmann C, Winkler E, Morin G, Kappler A. 2010. Anaerobic Fe(II)-oxidizing bacteria show As resistance and immobilize As during Fe (III) mineral precipitation. Environ Sci Technol 44:94–101.

Islam FS, Gault AG, Boothman C, Polya DA, Charnock JM, Chatterjee D, Lloyd JR. 2004. Role of metal-reducing bacteria in arsenic release from Bengal delta sediments. Nature 430:68–71.

Jiang J, Kappler A. 2008. Kinetics of microbial and chemical reduction of humic substances: Implications for electron shuttling. Environ Sci Technol 42:3563–3569.

Jones ME, Fennessey CM, DiChristina TJ, Taillefert M. 2010. Shewanella oneidensis MR-1 mutants selected for their inability to produce soluble organic-Fe(III) complexes are unable to respire Fe(III) as anaerobic electron acceptor. Environ Microbiol 12:938–950.

Kappler A, Brune A. 2002. Dynamics of redox potential and changes in redox state of iron and humic acids during gut passage in soil-feeding termites (*Cubitermes* spp.). Soil Biol Biochem 34:221–227.

Kappler A, Wuestner ML, Ruecker A, Harter J, Halama M, Behrens S. 2014. Biochar as electron shuttle between bacteria and Fe(III) minerals. Environ Sci Technol Lett 1:339–344.

Kendall B, Anbar A, Kappler A, Konhauser KO. 2012. The global iron cycle. In: Knoll AH, Canfield DE, Konhauser KO, editors. Fundamentals of Geobiology. New York: Wiley-Blackwell, p65–92.

Lalonde K, Mucci A, Ouellet A, Gelinas Y. 2012. Preservation of organic matter in sediments promoted by iron. Nature 483:198–200.

Lies DP, Hernandez ME, Kappler A, Mielke RE, Gralnick JA, Newman DK. 2005. Shewanella oneidensis MR-1 uses overlapping pathways for iron reduction at a distance and by direct contact under conditions relevant for biofilms. Appl Environ Microbiol 71:4414–4426.

Lohmayer R, Kappler A, Loesekann-Behrens T, Planer-Friedrich B. 2014. Role of sulfur species as redox partners and electron shuttles for ferrihydrite reduction by *Sulfurospirillum deleyianum*. Appl Environ Microbiol 80:3141–3149.

Lovley DR, Coates JD, Blunt-Harris EL, Phillips EJP, Woodward JC. 1996. Humic substances as electron acceptors for microbial respiration. Nature 382:445–448.

Lovley DR, Malvankar NS. 2015. Seeing is believing: novel imaging techniques help clarify microbial nanowire structure and function. Environ Microbiol DOI: 10.1111/1462-2920.12708

Lovley DR, Phillips EJP. 1988. Novel mode of microbial energy-metabolism-organic-carbon oxidation coupled to dissimilatory reduction of iron or manganese. Appl Environ Microbiol 54:1472–1480.

Luther III GW, Glazer BT, Ma SF, Trouwborst RE, Moore TS, Metzger E, Kraiya C, Waite TJ, Druschel G, Sundby B, Taillefert M, Nuzzio DB, Shank TM, Lewis BL, Brendel PJ. 2008. Use of voltammetric solid-state (micro)electrodes for studying biogeochemical processes: Laboratory measurements to real time measurements with an in situ electrochemical analyzer (ISEA). Mar Chem 108:221–235.

Luther III GW, Shellenbarger PA, Brendel PJ. 1996. Dissolved organic Fe(III) and Fe(II) complexes in salt marsh porewaters. Geochim Cosmochim Acta 60:951–960.

Marsili E, Baron DB, Shikhare ID, Coursolle D, Gralnick JA, Bond DR. 2008. Shewanella secretes flavins that mediate extracellular electron transfer. Proc Natl Acad Sci 105:3968–3973.

Melton ED, Swanner ED, Behrens S, Schmidt C, Kappler A. 2014. The interplay of microbially mediated and abiotic reactions in the biogeochemical Fe cycle. Nat Rev Microbiol 12:797–808.

Miot J, Benzerara K, Kappler A. 2014. Investigating microbe / mineral interactions: recent advances in X-ray and electron microscopies and redox-sensitive methods. Annu Rev Earth Planet Sci 42:271–289.

Muehe EM, Adaktylou IJ, Obst M, Zeitvogel F, Behrens S, Planer-Friedrich B, Kraemer U, Kappler A. 2013a. Organic carbon and reducing conditions lead to cadmium immobilization by secondary Fe

mineral formation in a pH-neutral soil. Environ Sci Technol 47:13430–13439.

Muehe EM, Obst M, Hitchcock A, Tyliszczak T, Behrens S, Schroeder C, Byrne JM, Michel FM, Kraemer U, Kappler A. 2013b. Fate of Cd during microbial Fe(III) mineral reduction by a novel and Cd-tolerant *Geobacter* species. Environ Sci Technol 47:14099–14109.

Muehe EM, Scheer L, Daus B, Kappler A. 2013c. Fate of arsenic during microbial reduction of biogenic versus abiogenic As–Fe(III)–mineral coprecipitates. Environ Sci Technol 47:8297–8307.

Myers CR, Nealson KH. 1988. Bacterial Manganese Reduction and Growth with Manganese Oxide as the Sole Electron Acceptor. Science 240:1319–1321.

Okamoto A, Hashimoto K, Nealson KH, Nakamura R. 2013. Rate enhancement of bacterial extracellular electron transport involves bound flavin semiquinones. Proc Natl Acad Sci 110:7856–7861.

Pearce CI, Wilkins MJ, Zhang C, Heald SM, Fredrickson JK, Zachara JM. 2012. Pore-scale characterization of biogeochemical controls on iron and uranium speciation under flow conditions. Environ Sci Technol 46(15):7992–8000.

Piepenbrock A, Dippon U, Porsch K, Appel E, Kappler A. 2011. Dependence of microbial magnetite formation on humic substance and ferrihydrite concentrations. Geochim Cosmochim Acta 75:6844–6858.

Pirbadian S, Barchinger SE, Leung KM, Byun HS, Jangir Y, Bouheni RA, Reed SB, Romine MF, Saffarini DA, Shi L, Gorby YA, Golbeck JH, El-Naggar MY. 2014. *Shewanella oneidensis* MR-1 nanowires are outer membrane and periplasmic extensions of the extracellular electron transport components. Proc Nat Acad Sci USA 111:12883–12888.

Porsch K, Dippon U, Rijal ML, Appel E, Kappler A. 2010. In-situ magnetic susceptibility measurements as a tool to follow geomicrobiological transformation of Fe minerals. Environ Sci Technol 44:3846–3852.

Porsch K, Rijal, M.L., Borch, T., Troyer, L.D., Behrens, S., Wehland, F., Appel, E., Kappler, A. 2014. Impact of organic carbon and iron bioavailability on the magnetic susceptibility of soils. Geochim Cosmochim Acta 128:44–57.

Posth NR, Canfield DE, Kappler A. 2014. Biogenic Fe(III) minerals: from formation to diagenesis and preservation in the rock record. Earth Sci Rev 135:103–121.

Raiswell R, Canfield DE. 2012. The iron biogeochemical cycle past and present. Geochem Persp 1(1):1–220.

Roden EE, Kappler A, Bauer I, Jiang J, Paul A, Stoesser R, Konishi H, Xu H. 2010. Extracellular electron transfer through microbial reduction of solid-phase humic substances. Nat Geosci 3:417–421.

Stookey L. 1970. Ferrozine - a new spectrometric reagent for iron. Anal Chem 42(7):779–781.

Taillefert M, Beckler JS, Carey E, Burns JL, Fennessey CM, DiChristina TJ. 2007. *Shewanella putrefaciens* produces an Fe(III)-solubilizing organic ligand during anaerobic respiration on insoluble Fe (III) oxides. J Inorg Biochem 101:1760–1767.

Taillefert M, Bono AB, Luther GW. 2000. Reactivity of freshly formed Fe(III) in synthetic solutions and (pore)waters: Voltammetric evidence of an aging process. Environ Sci Technol 34:2169–2177.

Taillefert M, Hover VC, Rozan TF, Theberge SM, Luther GW. 2002. The influence of sulfides on soluble organic-Fe(III) in anoxic sediment porewaters. Estuaries 25:1088–1096.

Tufano KJ, Fendorf S. 2008. Confounding impacts of iron reduction on arsenic retention. Environ Sci Technol 42:4777–4783.

Vaughan DJ, Lloyd JR. 2011. Mineral-organic-microbe interactions: Environmental impacts from molecular to macroscopic scales. Compt Rendus Geosci 343:140–159.

Veeramani H, Alessi DS, Suvorova EI, Lezama-Pacheco JS, Stubbs JE, Sharp JO, Dippon U, Kappler A, Bargar JR, Bernier-Latmani R. 2011. Products of abiotic U(VI) reduction by biogenic magnetite and vivianite. Geochim Cosmochim Acta 75:2512–2528.

Zachara JM, Kukkadapu RK, Fredrickson JK, Gorby YA, Smith SC. 2002. Biomineralization of poorly crystalline Fe(III) oxides by dissimilatory metal reducing bacteria (DMRB). Geomicrobiol J 19:179–207.